International Journal of Fracture 31 (1986) 211–231

Characteristics of an acoustic emission source from a thermal crack in glass

KWANG YUL KIM and WOLFGANG SACHSE

Department of Theoretical and Applied Mechanics, Cornell University, Ithaca, NY 14853, USA

(Received 10 October 1985)

Abstract.

Thermal cracks of mode I type oriented normal to the surface along an initial scratch were generated by blowing cold nitrogen gas through a small nozzle onto the surface of a glass plate. Acoustic emission (AE) signals emitted from the thermal cracks were detected on the opposite side of the plate, both at epicentral and at off-epicentral positions with a nine-channel AE system. AE source characteristics, such as moment tensor components, source-time function, radiation pattern, and dipole strength, were obtained from the detected waveforms. The strength of dipoles associated with the thermal cracks was determined from comparing the crack signals to those generated when a glass capillary was broken at the crack site prior to crack formation. It is shown that the AE source-time function, together with the dipole strength, can provide valuable information on the dynamic behavior of fracture.

1. Introduction

Successful implementation of acoustic emission (AE) techniques used for in situ structural integrity monitoring applications depends on correct identification of the type of AE source, such as the formation of a crack. In this paper, recent developments in the area of source representation in the case of a seismic faulting [1] and in the case of indentation cracks [2,3] of mode I type generated in glass, have been successfully applied to the study of AE sources from thermal cracks generated on the surface of soda-lime glass plate.

The propagation of transient elastic waves in the bounded medium was investigated in detail by Knopoff [4], Hsu et al. [5], and Pao and his coworkers [6,7], and their results are utilized to remove the effect of the structure on the detected AE signals.

Although determination of moment tensor components and time behavior for the characterization of the AE source was previously carried out by the authors for the case of penny-shaped indentation cracks [2,3] in glass, the determination of the absolute magnitude of the components of the moment tensor was left unresolved. In the study of thermal cracks we extend our previous work to include the determination of absolute magnitude of the components of the moment tensor. This, together with the source-time function and the measured crack size, will completely characterize the AE source and can lead to important information on the fracture dynamics of crack formation.

2. Experiment

The specimen used for thermal crack generation was a soda-lime glass plate which was 1.86 cm thick, about 16 cm wide, and 16 cm long. On one side of the plate, a fine, shallow

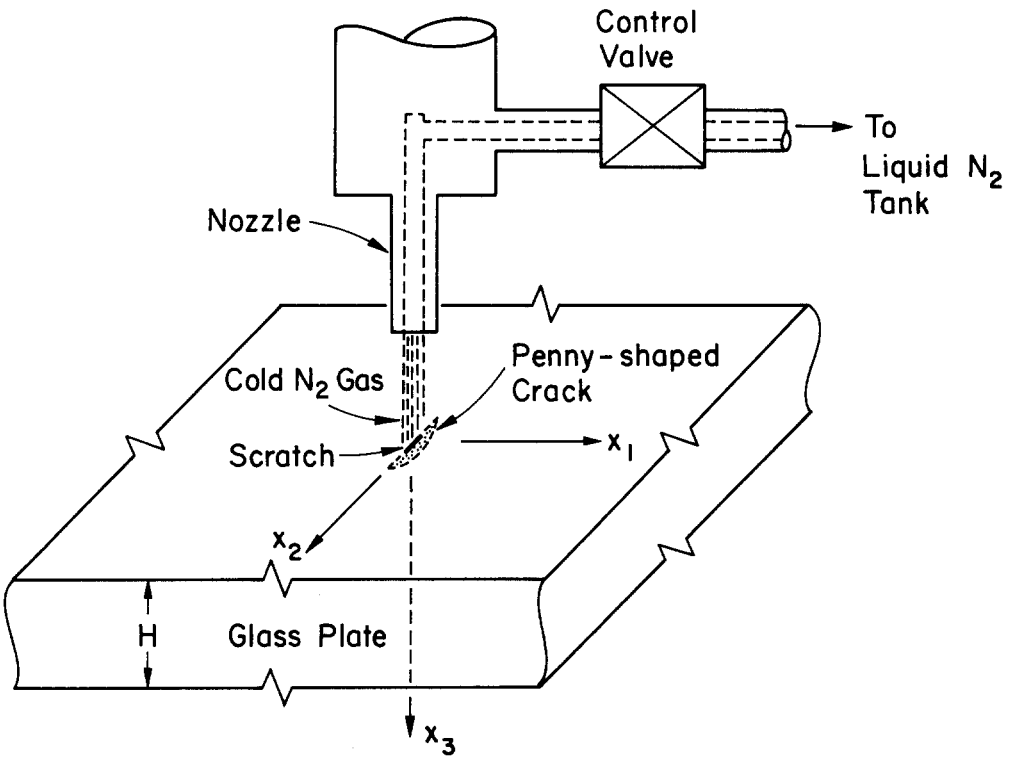

Figure 1. Schematics of thermal crack generation in a glass plate.

scratch of ~ 1 mm length was drawn by using a glass cutter wheel at the site where a crack was to be generated by cooling. The scratch served as a preferred nucleation site for crack generation. As shown in Fig. 1, cold nitrogen gas was blown through a small nozzle of 1.5 mm diameter onto the surrounding area of the scratch via a fine control valve connected to a liquid nitrogen tank. Care was taken to ensure as symmetric cooling around the scratch as possible. The control valve was used to control the cooling rate for optimization of small, fine crack generation. This was achieved by trial and error. No effort has been made to measure cooling rate or surface temperature of the cooled spot.

As the cooling proceeded, it was repeatedly observed that a thermal crack was suddenly generated from the scratch site, extending both downwards and sideways along the scratch direction. The generated crack generally resembled a sectioned penny. The formation and growth of thermal cracks were monitored by the AE sensors located on the opposite side of the plate from the AE source. As soon as AE signals associated with crack formation were detected, the control valve was shut and cooling stopped. The typical dimension of the generated thermal cracks was observed to be about 4 mm sideways and 1 mm downwards.

Figure 2 shows the locations of nine AE sensors used in the experiment. At epicenter is a capacitive transducer to detect normal displacement and at a distance of 2.07 H from epicenter are eight piezoelectric pinducers whose angular coordinates are indicated in the figure. The detector side of the glass plate was coated with a 0.5 μm thick chromium film and connected to the ground. The electronic block diagram for the data acquisition is displayed in Fig. 3. The signals detected by the epicentral capacitive transducer are first amplified by a charge amplifier which has a bandwidth from 10 kHz to over 10 MHz and a sensitivity of 0.25 volt per picofarad. The output of the charge amplifier is then

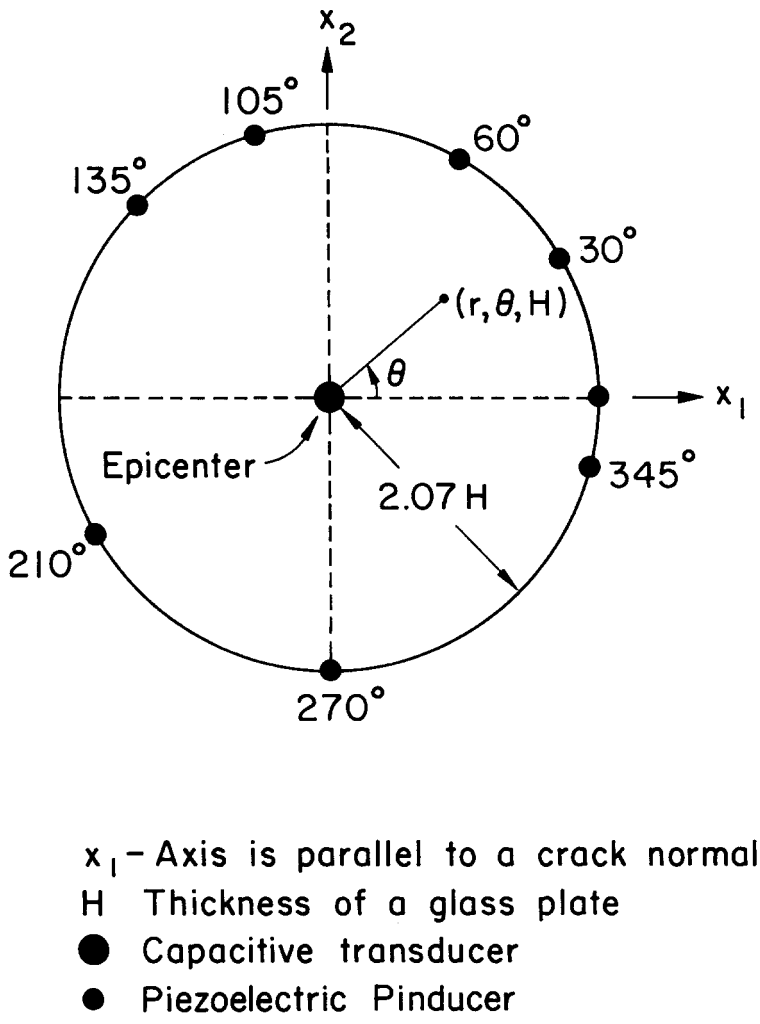

Figure 2. Locations of AE sensor used in the experiment.

connected to an eight-bit transient recorder which also serves as an external trigger source for the other eight transient recorders. These were used to record the amplified output of the off-epicentral, piezoelectric transducer signals. The bandwidth of the preamplifier is from ~ 10 kHz to ~ 2 MHz and a gain of 60 db was used. The crack signals recorded by the transient recorders were brought into a digital computer for subsequent signal processing and data reduction. There was provision for the storage of both the detected AE signals and processed data.

Prior to the crack formation, a glass capillary which had 0.05 mm inside diameter and 0.08 mm outside diameter was broken at the intended site of crack generation by pressing it vertically on the surface with a razor blade via a miniature load cell. A strength of capillary fracture was measured by the load cell. The description of this apparatus is already reported elsewhere [8]. Thermal crack generation was immediately induced to minimize any disturbance of the whole measurement system. The purpose of the capillary fracture, which generates an axisymmetric AE signal, is two-fold: first, to compensate for the effects of both variable sensitivities of different pinducers and their couplants on the detected AE signals; second, to measure the breaking strength of capillary fracture which

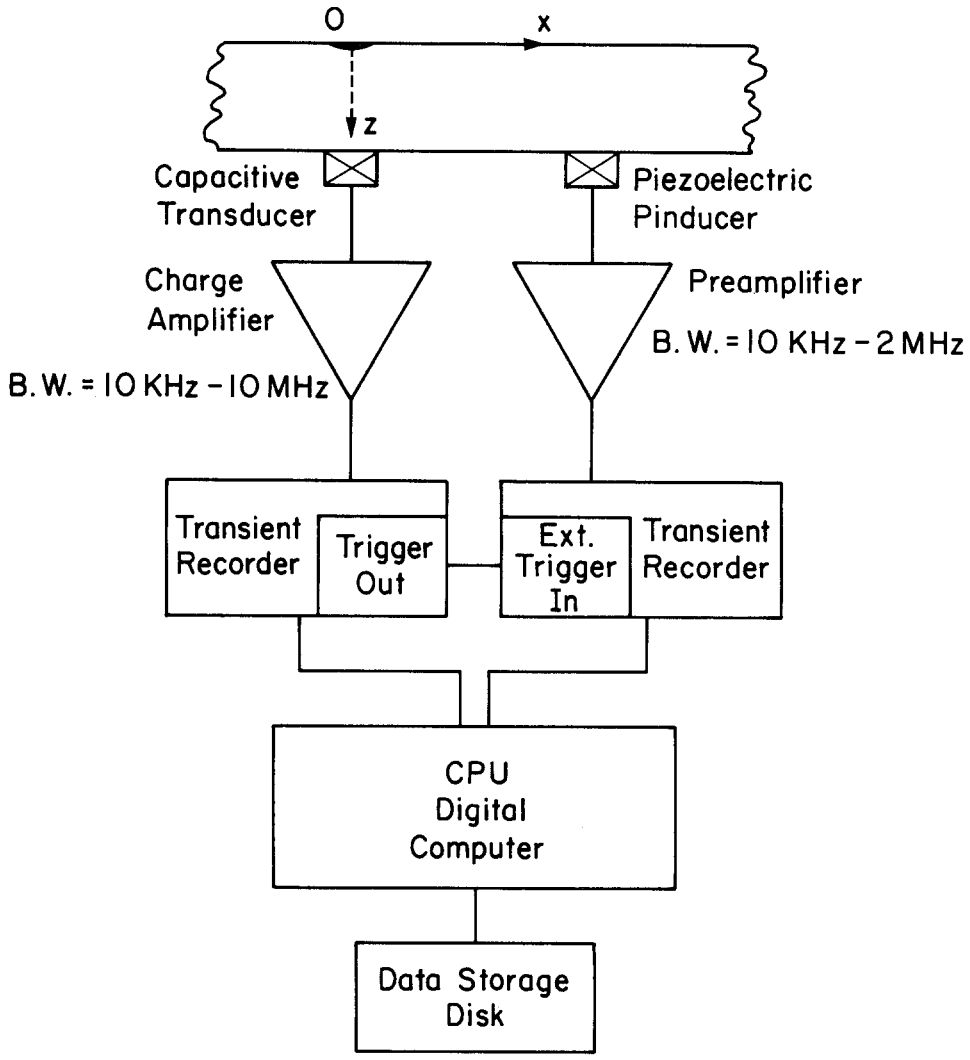

Figure 3. Electronic block diagram of an AE system.

is later used in the calculation of the dipole strength of a thermal crack. These are explained in detail in the following sections.

3. Theory

3.1. General considerations

Consider a stress present on a very shallow hypothetical crack plane lying normal to a surface which is kept traction-free as shown in Fig. 1. Because of a free boundary, the stress components acting on the theoretical crack plane, σ_{33}, σ_{23}, and σ_{31}, are all virtually equal to zero. Furthermore, if the condition of symmetric cooling about the scratch is nearly satisfied, $\sigma_{12} \approx 0$ [9]. Since all the shear stress components on the crack plane identically vanish, thermal cracks generated under symmetric cooling are of mode I type, according to the usual definition in fracture mechanics.

The AE source representation of these thermal cracks is equivalent to that of a penny-shaped crack advancing from the surface inward in a two-dimensional thin plate, while propagation of their AE signals in the glass plate is three-dimensional in nature. An AE source whose dimension is reasonably smaller than the dominant wavelength of the generated AE and much smaller than the distance between the source and the receiver can be treated as a point source. The size of a shallow thermal crack extending sideways ~ 4 mm on the surface is comparable to the dominant wavelength of *P*-wave (5.8 mm at 1 MHz frequency) and should be treated as an extended AE source in a strict sense. However, it is assumed here that it can be treated as a point source. This assumption has turned out to be quite successful in describing both the waveforms detected by the AE sensors and the radiation patterns, as will be shown in Section 4. Hence our theory and analysis of experimental data will be based on this point source representation as an AE source for the thermal cracks.

3.2. AE moment tensor

Since Gilbert's [10] introduction of the concept of moment tensor, it has been investigated in detail to represent different types of seismic sources [1,11,12,13]. Pao and his collaborators [6,7] extended his concept of the moment tensor to the study of acoustic emission to accommodate various types of AE sources which were illustrated in Love's book [14]. From a practical point of view, the utility of the moment tensor representation lies in the fact that it is general, that is, it can accommodate different types of sources, and that the response to these sources is linearly related to them.

A displacement $\boldsymbol{u}(\boldsymbol{x}, t)$ at location $\boldsymbol{x}$ at time t due to $f(\boldsymbol{\xi}, t)$, the causal excitation function in a region V, can be expressed by means of Green's functions [1,15]:

$$u_i(\boldsymbol{x}, t) = \int_0^t \int_V G_{ji}(\boldsymbol{x}, \boldsymbol{\xi}; t-\tau) f_j(\boldsymbol{\xi}, \tau)\, \mathrm{d}V\, \mathrm{d}\tau. \tag{3.1}$$

In this equation and those following, the summation over the repeated indices is implied unless otherwise specified. If the excitation force acts in a small source volume, which can be replaced by a point source about some reference point $\boldsymbol{\xi}^0$, the Green's function can be expanded in a Taylor series about $\boldsymbol{\xi}^0$ to obtain

$$\begin{aligned} u_i(\boldsymbol{x}, t) = {} & \int_0^t \mathrm{d}\tau G_{ji}(\boldsymbol{x}, \boldsymbol{\xi}^0; t-\tau) \int_V f_j(\boldsymbol{\xi}, \tau)\, \mathrm{d}V \\ & + \int_0^t \mathrm{d}\tau \frac{\partial}{\partial \xi_k} G_{ji}(\boldsymbol{x}, \boldsymbol{\xi}^0; t-\tau) \int_V (\xi_k - \xi_k^0) f_j(\boldsymbol{\xi}, \tau)\, \mathrm{d}V \\ & + \int_0^t \mathrm{d}\tau \frac{\partial^2 G_{ji}}{\partial \xi_k \partial \xi_l} \int_V (\xi_k - \xi_k^0)(\xi_l - \xi_l^0) f_j(\boldsymbol{\xi}, \tau)\, \mathrm{d}V \\ = {} & u_i^m(\boldsymbol{x}, t) + u_i^d(\boldsymbol{x}, t) + \ldots . \end{aligned} \tag{3.2}$$

$u_i^m(\boldsymbol{x}, t)$ in (3.2) is due to the monopole contribution:

$$u_i^m(\boldsymbol{x}, t) = F_j(\boldsymbol{\xi}^0, t) * G_{ji}(\boldsymbol{x}, \boldsymbol{\xi}^0; t), \tag{3.3}$$

where

$$F_j(\boldsymbol{\xi}^0, \tau) = \int_V f_j(\boldsymbol{\xi}, \tau)\, \mathrm{d}V \tag{3.4}$$

is the total force acting in the volume V with its moment equal to zero and $*$ denotes a convolution integral in time. $u_i^d(\boldsymbol{x}, t)$ in (3.2) is expressed as

$$u_i^d(\boldsymbol{x}, t) = M_{jk}(\boldsymbol{\xi}^0, t) * G_{ji,k}(\boldsymbol{x}, \boldsymbol{\xi}^0; t). \tag{3.5}$$

It represents the contribution to the force moment tensor M_{jk} of spatial degree one:

$$M_{jk}(\xi^0, \tau) = \int_V (\xi_k - \xi_k^0) f_j(\xi, \tau)\, dV. \tag{3.6}$$

The force moment tensor M_{jk} in (3.6) is usually referred to as a double force in the j-th direction when $j = k$ (no summation implied) and a single couple when $j \neq k$. As a whole, it is simply referred to as a dipole source term. Likewise, $G_{ji,k}(x, \xi^0; t) \equiv \frac{\partial}{\partial \xi_k} G_{ji}(x, \xi^0; t)$ in (3.5) is called a dipole Green's function. Bachus [16] demonstrated that in the seismic faulting of a small volume, only force moments less than a few degrees in (3.2) are needed to describe the response due to the source excitation.

Equation (3.3) can be used to describe a response from monopole sources with zero force moment, such as pencil-lead breaking and glass capillary fracture [5]. If the excitation is caused not by external forces but by the failure of the material such as the formation of the thermal cracks described in Section 2, the force and its moment must be self-equilibrating in the source region. Therefore, there can be no monopole contribution and (3.5) describes the displacement resulting from an AE source associated with thermal crack generation with the property that its moment tensor is symmetric, i.e., $M_{jk} = M_{kj}$.

As described earlier in this section, there is no shear stress contribution to the formation of a mode I crack. Consequently, the off-diagonal elements of the moment tensor $M_{jk}(j \neq k)$ are all equal to zero for mode I cracks. Furthermore, for thermal cracks mentioned above, $\sigma_{33} = 0$ and likewise $M_{33} = 0$. Thus, the moment tensor $\boldsymbol{M}$ associated with a thermal crack AE source can be written in matrix form:

$$\boldsymbol{M}(t) = \begin{bmatrix} M_{11}(t) & 0 & 0 \\ 0 & M_{22}(t) & 0 \\ 0 & 0 & 0 \end{bmatrix}. \tag{3.7}$$

Note that the form of the moment tensor above is that of a mode I crack in a two-dimensional thin plate.

If the thermal cracks generated are of mixed type with the shear stress σ_{12} present, the moment tensor in (3.7) is modified and written as

$$\boldsymbol{M} = \begin{bmatrix} M_{11}(t) & M_{12}(t) & 0 \\ M_{21}(t) & M_{22}(t) & 0 \\ 0 & 0 & 0 \end{bmatrix}. \tag{3.8}$$

The time function associated with $M_{ij}(t)$ is primarily governed by the crack velocity. The assumption is made that all the elements of the moment tensor $M_{ij}(t)$ associated with the same thermal crack share the same time function which we denote by $S(t)$. For AE sources associated with cracks, $S(t)$ is generally known to be step-like, similar to characteristics of a Heaviside step-, a linear ramp-, or a parabolic ramp-function, but it is at this stage an unknown time function controlled by the energetics of crack formation. We will normalize the step-like $S(t)$ with risetime Δ and will denote it by $\hat{S}^d(t)$ which has unit amplitude when $t \gg \Delta$. Writing $M_{ij}(t) = D_{ij}\hat{S}^d(t)$ when $i = j$ and $M_{ij}(t) = C_{ij}\hat{S}^d(t)$ when $i \neq j$, (3.8) can be expressed as

$$\boldsymbol{M} = \begin{bmatrix} D_{11} & C_{12} & 0 \\ C_{12} & D_{22} & 0 \\ 0 & 0 & 0 \end{bmatrix} \hat{S}^d(t). \tag{3.9}$$

D_{11} and D_{22} are known as the strength of dipoles, and C_{12} is called the strength of a single couple. Our purpose for the characterization of an AE source of the thermal crack is to determine D_{11}, D_{22}, C_{12}, and $\hat{S}^d(t)$.

3.3. AE radiation pattern

In this subsection we will pay particular attention to the radiation pattern of the AE signals detected by the off-epicentral transducers shown in Fig. 2.

Let the typical receiver location x^0 be denoted by the polarcylindrical coordinate, $r = 2.066\,H$, θ, H, where H is the thickness of the glass plate and θ is an angle measured from the crack normal parallel to the x_1-axis. Then, the normal displacement $u_3^d(x^0, t)$ resulting from the AE source described by (3.9) is obtained by substituting (3.9) into (3.5):

$$u_3^d(x^0, t) = \hat{S}^d(t) * \{ D_{11} G_{13,1}(x^0, \xi^0; t) + D_{22} G_{23,2}(x^0, \xi^0; t) + C_{12}[G_{13,2}(x^0, \xi^0; t) + G_{23,1}(x^0, \xi^0; t)] \}. \tag{3.10}$$

Applying the generalized ray theory to an infinite elastic plate [6,7], the convolution integrals in (3.10) can be seen to have an angular dependence of the form

$$\begin{aligned} &\hat{S}^d(t) * G_{13,1}(x^0, \xi^0; t) = g(t) \cos^2\theta, \\ &\hat{S}^d(t) * G_{23,2}(x^0, \xi^0; t) = g(t) \sin^2\theta, \\ &\hat{S}^d(t) * G_{13,2}(x^0, \xi^0; t) = h(t) \sin 2\theta = \hat{S}^d(t) * G_{23,1}(t), \end{aligned} \tag{3.11}$$

where $g(t)$ and $h(t)$ are both functions of time, independent of θ.

Substitution of (3.11) into (3.10) yields the radiation pattern

$$u_3^d(t) = d(t)(\cos^2\theta + b) + c(t) \sin 2\theta, \tag{3.12}$$

where

$$b = \frac{D_{22}}{D_{11} - D_{22}}, \tag{3.13}$$

$$d(t) = (D_{11} - D_{22}) g(t), \quad c(t) = 2C_{12} h(t). \tag{3.14}$$

The radiation pattern was determined from the peak amplitude of the first P-ray of the crack signals detected by the pinducers. In order to eliminate the effects of both the transducer couplants and differing sensitivities of various pinducers on the measured amplitude of detected signals, the first P-wave amplitude of the crack signal was normalized against the corresponding amplitude of glass capillary fracture which was performed immediately before thermal crack generation, as mentioned in Section 2. The type of AE point transducer has been observed to be principally sensitive to normal velocity of surface motion. However, it is assumed that the normalized, P-wave amplitude is proportional to the surface displacement. A linear least squares method was used to fit these normalized P-wave amplitude data into a form of (3.12) to determine the coefficients d, b, and c.

3.4. The strength of dipoles

The strength of dipoles was determined by comparing the epicentral normal displacement response due to crack formation with that due to glass capillary fracture, utilizing the fact that at epicenter contributions of single couple source terms to normal displacements vanish and $\hat{S}^d(t) * G_{13,1}(t) = \hat{S}^d(t) * G_{23,2}(t)$. Let $\hat{u}_3^m$ and $\hat{u}_3^d$ represent, respectively, the nondimensional, normalized displacements at epicenter for the step-like source-time functions of unit magnitude, $\hat{S}^m(t)$ and $\hat{S}^d(t)$. $\hat{S}^m(t)$ is the source-time function associated with the capillary fracture. Similarly, V_0^m and V_0^d are the corresponding outputs of the charge amplifier and u_3^m and u_3^d denote the corresponding surface

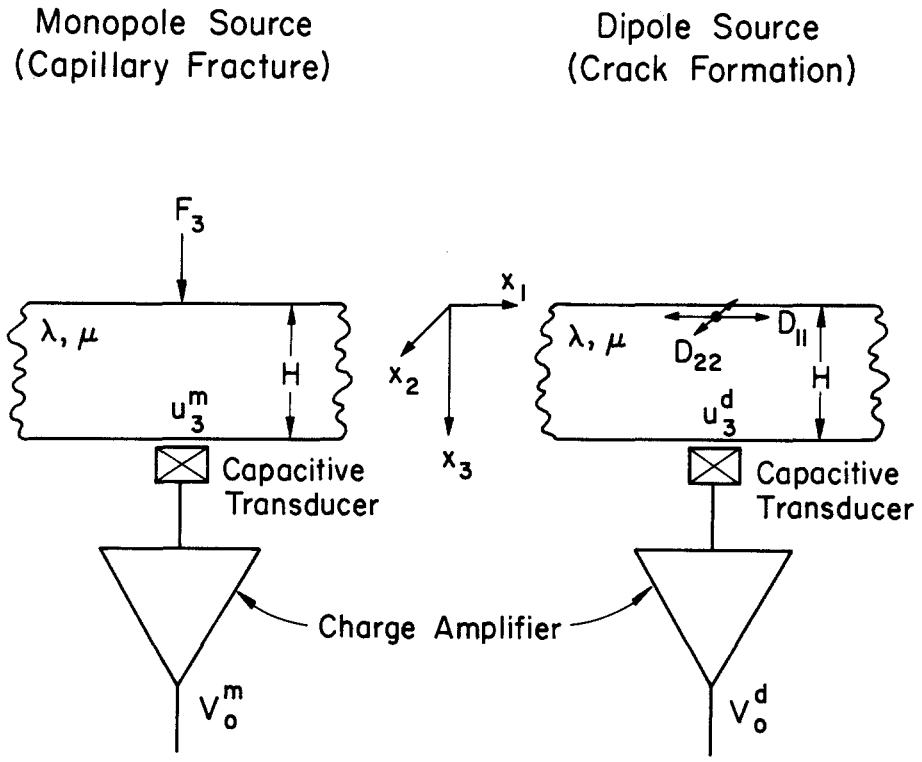

Figure 4. Diagram indicating the configuration of monopole and dipole sources, and epicentral receivers.

displacements at epicenter. Referring to Fig. 4, Fig. 5, and the work of Ceranoglu and Pao [7], one obtains

$$V_0^m(t) = ku_3^m(t) = \frac{kF_3}{\pi\mu H}\hat{u}_3^m(t) = kF_3\hat{S}^m(t) * G_{33}(t), \tag{3.15}$$

$$V_0^d(t) = ku_3^d(t) = \frac{k(D_{11}+D_{22})}{\pi\mu H^2}\hat{u}_3^d(t) = k(D_{11}+D_{22})\hat{S}^d(t) * G_{13,1}(t), \tag{3.16}$$

where k is a constant independent of time, μ is the shear modulus of the specimen, and F_3 is the strength of capillary fracture. With both $V_0^m(t)$ and $V_0^d(t)$ measured, and $G_{33}(t)$ and $G_{13,1}(t)$ theoretically calculated, $kF_3\hat{S}^m(t)$ and $k(D_{11}+D_{22})\hat{S}^d(t)$ can now be calculated by the method of deconvolution:

$$kF_3\hat{S}^m(t) = V_0^m * [G_{33}]^{-1}, \tag{3.17}$$

$$k(D_{11}+D_{22})\hat{S}^d(t) = V_0^d * [G_{13,1}]^{-1}. \tag{3.18}$$

Noticing that both $\hat{S}^m(t)$ and $\hat{S}^d(t)$ approach unity when $t \gg \Delta$ (risetime), one obtains

$$D_{11}+D_{22} = F_3\frac{\left\{V_0^d * [G_{13,1}]^{-1}\right\}_{t\gg\Delta_d}}{\left\{V_0^m * [G_{33}]^{-1}\right\}_{t\gg\Delta_m}}. \tag{3.19}$$

The above equation, simple as it appears, is not used for the determination of $(D_{11}+D_{22})$. It is prone to numerical errors introduced in the deconvolution process. Instead, the ensuing approach is to calculate $\hat{u}_3^m(t)$ from $\hat{S}^m(t)$ and $\hat{u}_d(t)$ from $\hat{S}^d(t)$, where $\hat{S}^m(t)$

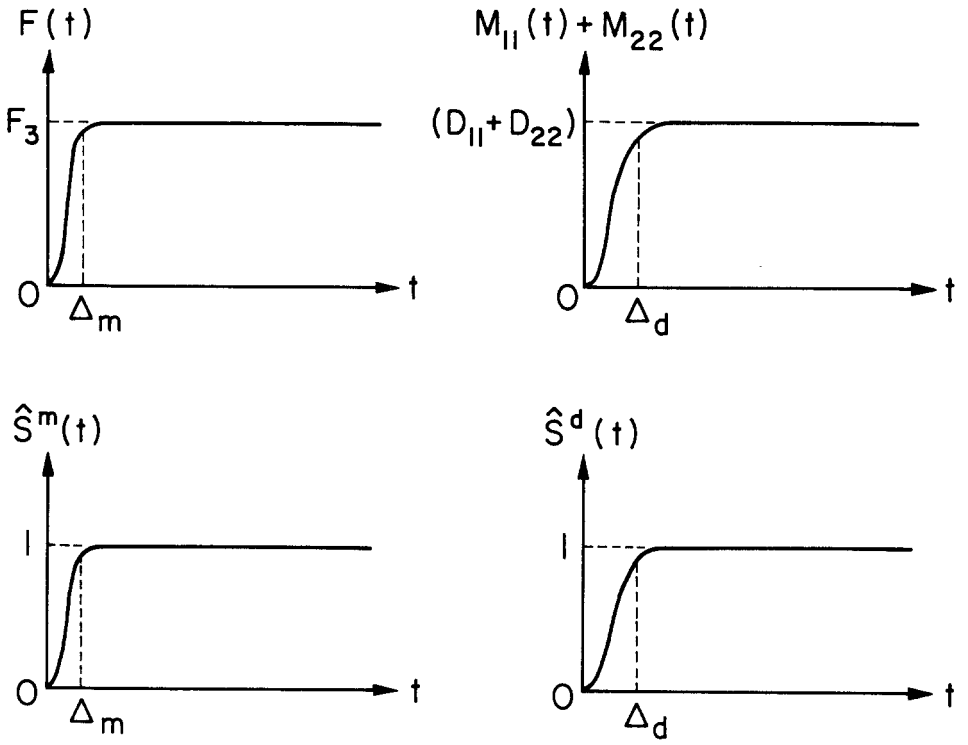

Figure 5. Schematics of monopolar and dipolar sourcetime functions.

and $\hat{S}^d(t)$ are easily obtained by normalizing (3.17) and (3.18), respectively. Dividing (3.16) by (3.15) yields

$$D_{11} + D_{22} = F_3 H \left[\frac{\hat{u}_3^m}{V_0^m} \right] \left[\frac{\hat{u}_3^d}{V_0^d} \right]^{-1}. \tag{3.20}$$

The ratio in each square bracket in (3.20) was determined by averaging the values over a time interval 6 μsec beginning from the first P-wave arrival.

The magnitudes of both D_{11} and D_{22} were obtained from (3.13) and (3.20):

$$D_{11} = \frac{1+b}{1+2b} F_3 H \left[\frac{\hat{u}_3^m}{V_0^m} \right] \left[\frac{V_0^d}{\hat{u}_3^d} \right], \tag{3.21}$$

$$D_{22} = \frac{b}{1+b} D_{11}. \tag{3.22}$$

The magnitude of C_{12} in (3.9) can be obtained by calculating the offepicentral response at the pinducer location. However, it turned out to be unnecessary because all the thermal cracks generated were essentially mode I cracks, as demonstrated in the next section.

4. Experimental data and results

Typical AE signals of glass thermal cracks (GTC) detected by the various piezoelectric pinducers and the capacitive transducer are displayed in Fig. 6(a) for GTC 05. The corresponding AE signals of glass capillary breaking (GCB) are shown in Fig. 6(b).

As discussed in the previous section, the 1P-wave amplitude data for crack signals normalized to those of a breaking glass capillary were fit into a form of (3.12) to

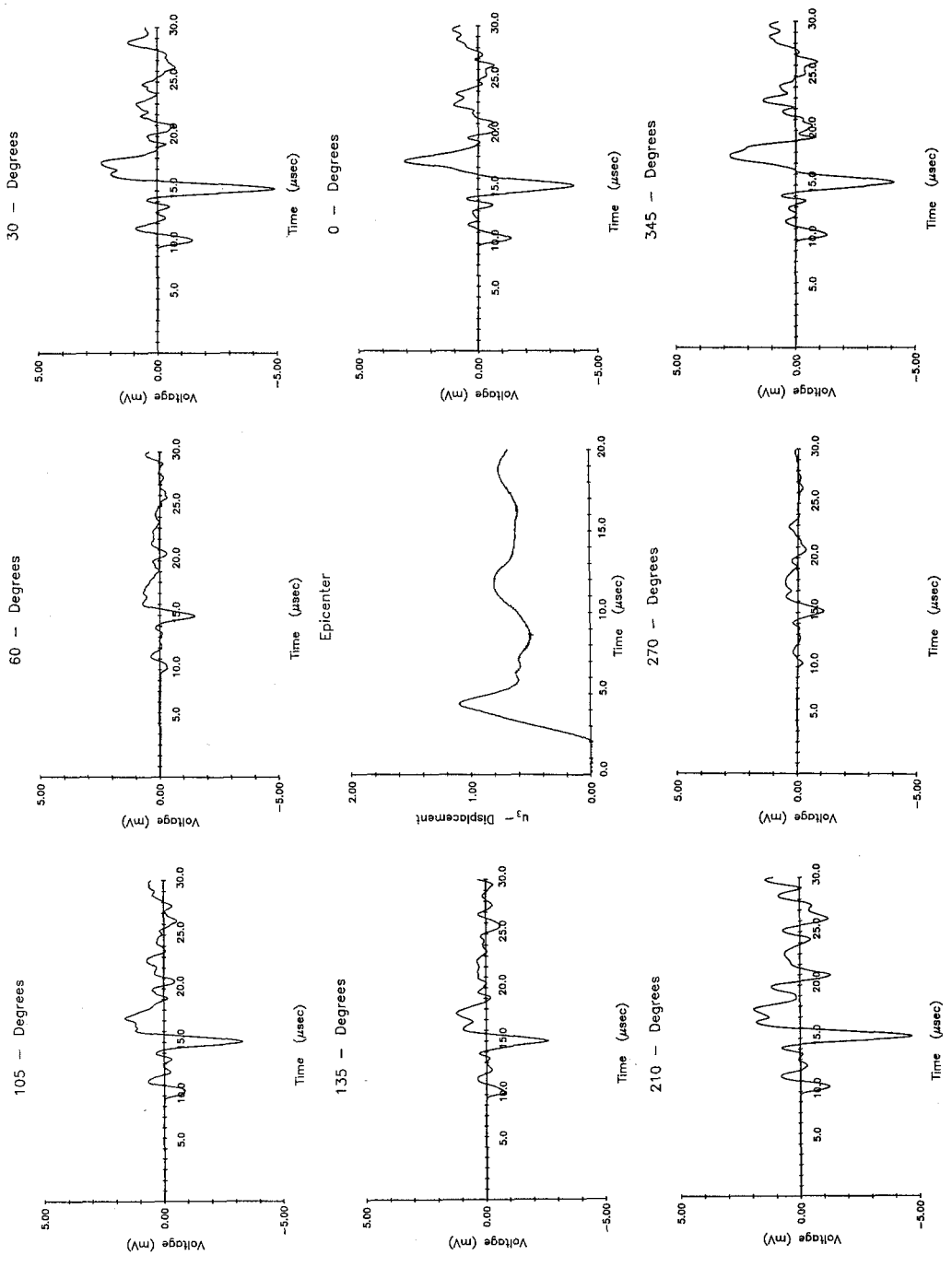

Figure 6(a). Detected AE signals from glass thermal crack, GTC 05.

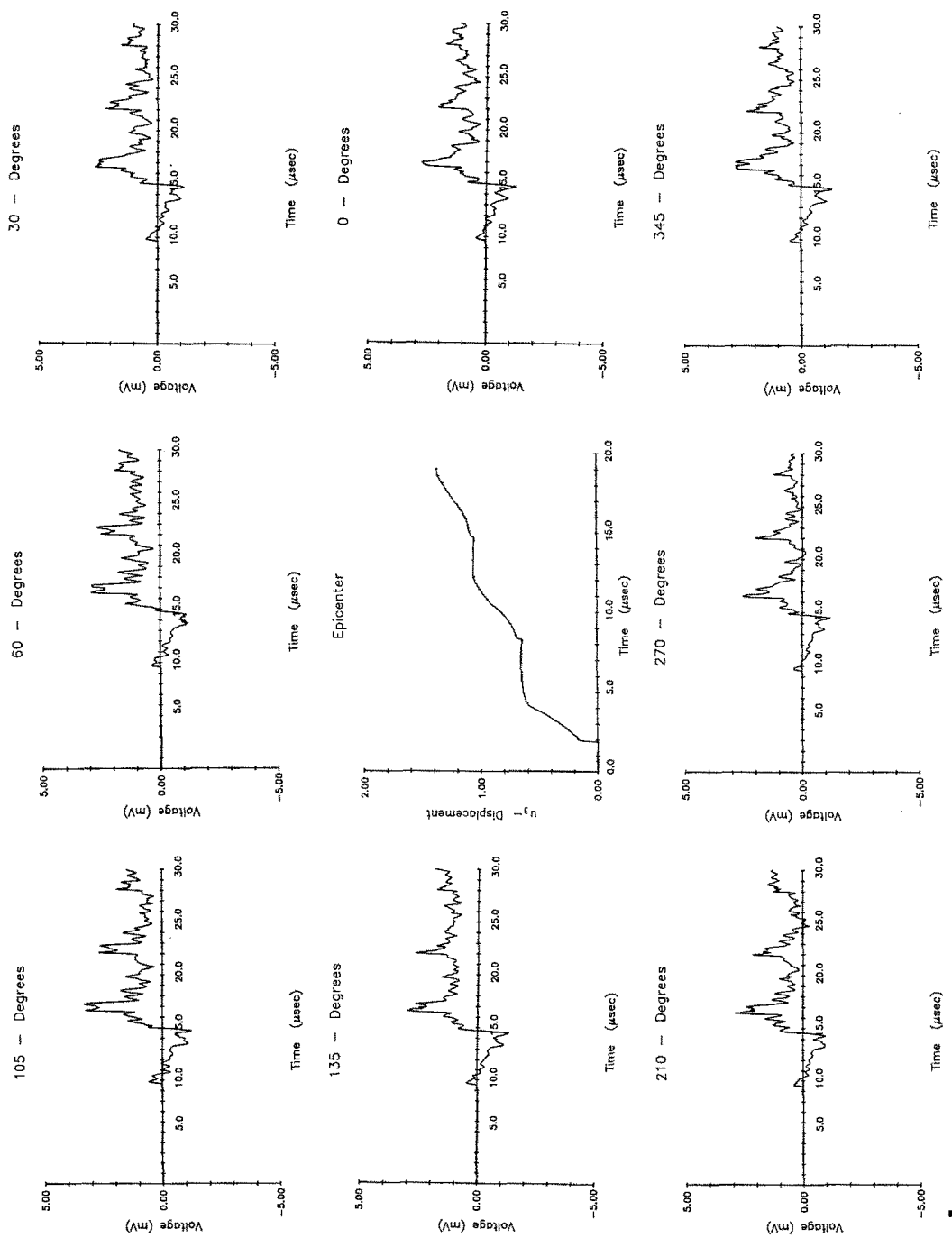

Figure 6(b). Corresponding AE signals from glass capillary fracture.

Table 1. Relevant data for determination of AE source characteristics of Glass Thermal Cracks (GTC)

Crack no.	Radiation pattern parameter (b)	Strength of capillary fracture (F_3N-m)	$\left[\frac{\hat{u}_3^m}{V_0^m}\right]^*$	$\left[\frac{\hat{u}_3^d}{V_0^d}\right]^*$
GTC 01	0.116			
GTC 02	−0.062			
GTC 03	0.080	2.07	1.699	6.822
GTC 04	0.113	1.98	2.200	1.331
GTC 05	0.030	2.77	3.907	2.967
GTC 06	0.105	2.47	2.519	1.935
GTC 07	0.041	2.76	2.224	2.132
GTC 08	0.166	2.59	1.802	1.287
GTC 09	0.038	2.80	2.903	3.101
GTC 10	0.087	2.49	3.484	1.263
GTC 11	0.141	2.97	1.112	1.706

* cf. Eqn. (3.20)

determine the θ-independent constants d, b, and c. The results of curve-fitting by the linear least squares method for eleven different thermal cracks listed in Table 1 showed that $c \ll d$ and $c < 2\sigma$, where σ is the standard deviation associated with c. This essentially verifies that all of the thermal cracks generated are of mode I type, and the strength of a single couple C_{12} in (3.9) is zero for all cracks. These results would be expected from the symmetric cooling around the scratch. The values of b are recorded in Table 1, while those of D_{22}/D_{11} calculated from (3.13) are listed in Table 2. Typical radiation patterns generated from these constants are plotted in Figs. 7(a) and 7(b) for two different cracks. It is noted that D_{22}/D_{11} is generally small, typically around 0.1 or less.

It has been deduced on the basis of the free boundary condition that the moment tensor component M_{33} (or D_{33}) should be zero. In order to verify this, the epicentral response is written in the form

$$u_3^d(t) = D_{11}\hat{S}^d(t) * [G_{13,1}(t) + r_2 G_{23,2}(t) + r_3 G_{33,3}(t)]$$
$$= D_{11}(1 + r_2)\hat{S}^d(t) * [G_{13,1}(t) + aG_{33,3}(t)], \tag{4.1}$$

Table 2. AE source characteristics of Glass Thermal Cracks (GTC)

Crack no.	Component of moment tensor		Source-time function	
	D_{22}/D_{11}	D_{33}/D_{11} *	Strength of a normal dipole ($D_{11}N-m$)	Risetime (μsec)
GTC 01	0.104	0(0.003)		
GTC 02	−0.066	0(0.002)		
GTC 03	0.074	0(0.004)	8.90×10^{-3}	0.32
GTC 04	0.102	0(−0.011)	5.52×10^{-2}	0.80
GTC 05	0.029	0(0.027)	6.59×10^{-2}	1.12
GTC06	0.095	0(−0.034)	5.45×10^{-2}	1.05
GTC 07	0.039	0(0.002)	5.15×10^{-2}	0.70
GTC 08	0.142	0(0.011)	5.89×10^{-2}	0.96
GTC 09	0.037	0(−0.023)	4.70×10^{-2}	0.64
GTC 10	0.080	0(0.063)	1.18×10^{-1}	1.75
GTC 11	0.124	0(0.001)	3.20×10^{-2}	0.80

* The values in parentheses are the results of signal processing

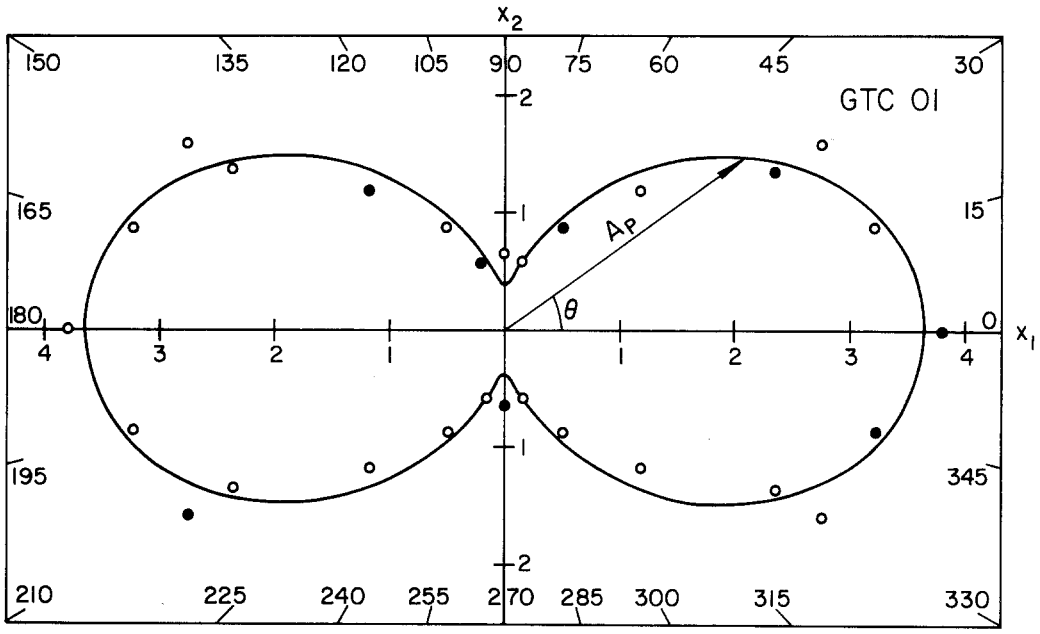

a •- Real Data Points, o- Images across x_1, x_2 Axes; $A_P=3.27\,(0.116+\cos^2\theta)$

x_1- Axis parallel to a Normal to the Crack Plane

Figure 7(a). Radiation pattern of AE signals from GTC 01.

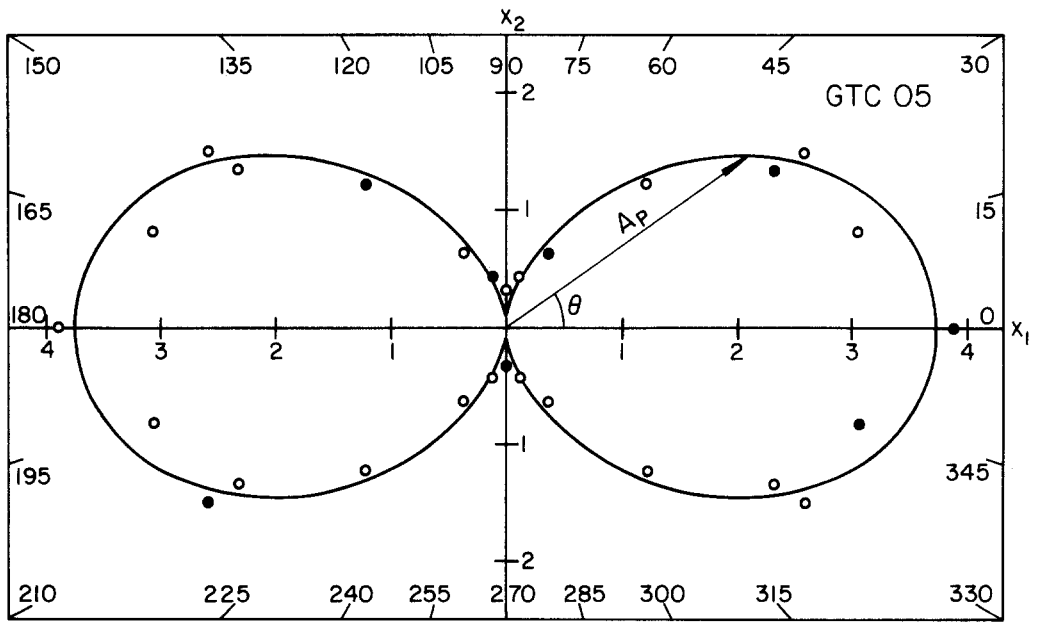

b •- Real Data Points, o- Images across x_1, x_2 Axes; $A_P=3.65\,(0.030+\cos^2\theta)$

x_1- Axis parallel to a Normal to the Crack Plane

Figure 7(b). Radiation pattern of AE signals from GTC 05.

where

$$r_2 \equiv D_{22}/D_{11}, \quad r_3 \equiv D_{33}/D_{11}, \tag{4.2}$$

and

$$a \equiv \frac{r_3}{1+r_2} = \frac{D_{33}}{D_{11}+D_{22}}. \tag{4.3}$$

The observed epicentral signals were deconvolved with the theoretically calculated Green's functions to determine both $\hat{S}^d(t)$ and a in (4.1). A double iterative, least-squares signal processing algorithm [17] was used for this purpose. The values of a turned out to be so small for all the thermal cracks, except for GTC 10, as to be physically meaningless (see Table 2), and they are less than the errors resulting from signal processing, which are typically a few percent. Thus, the result of the signal processing proves our logical deduction that there can be no dipole component normal to a free boundary for an AE source which is located either at the boundary or very near it. The values of D_{33}/D_{11} were calculated from (4.3) and (3.13), ignoring the negligible effect of D_{33} on b appearing in (3.12). They are recorded for reference in parentheses in Table 2.

The normalized dipole source functions, $\hat{S}^d(t)$, are exhibited in Figs. 8(a) and 8(b) for GTC 04 and GTC 05, respectively. Risetime data measured from $\hat{S}^d(t)$ are also listed in Table 2.

The location of the point source of AE signals for all cracks is given the coordinate (0, 0, 0.01H), as the cracks penetrate slightly below the surface. The speeds of P-wave (C_p) and S-wave (C_s) necessary for the calculation of the plate Green's functions were experimentally measured. They were

$$C_p = 0.582 \text{ cm}/\mu\text{sec}, \quad C_s = 0.350 \text{ cm}/\mu\text{sec}. \tag{4.4}$$

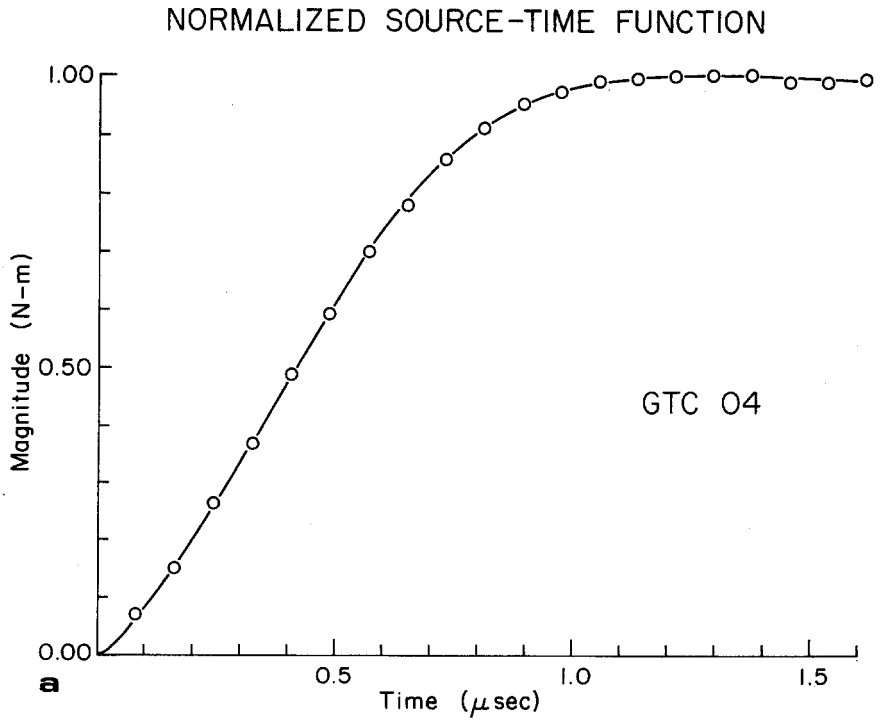

Figure 8(a). Normalized source-time function of GTC 04.

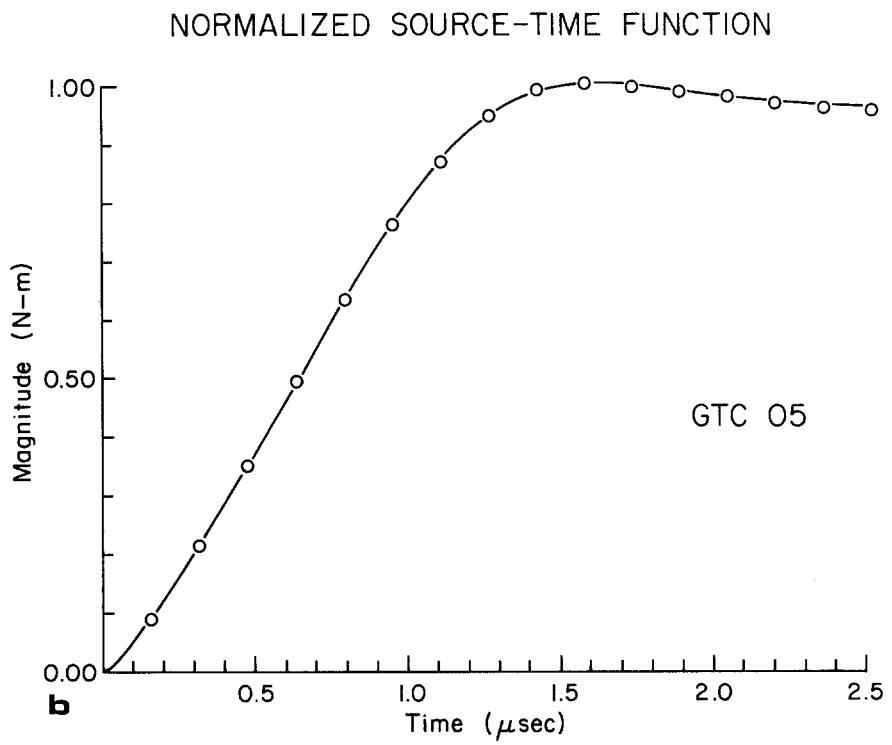

Figure 8(b). Normalized source-time function of GTC 05.

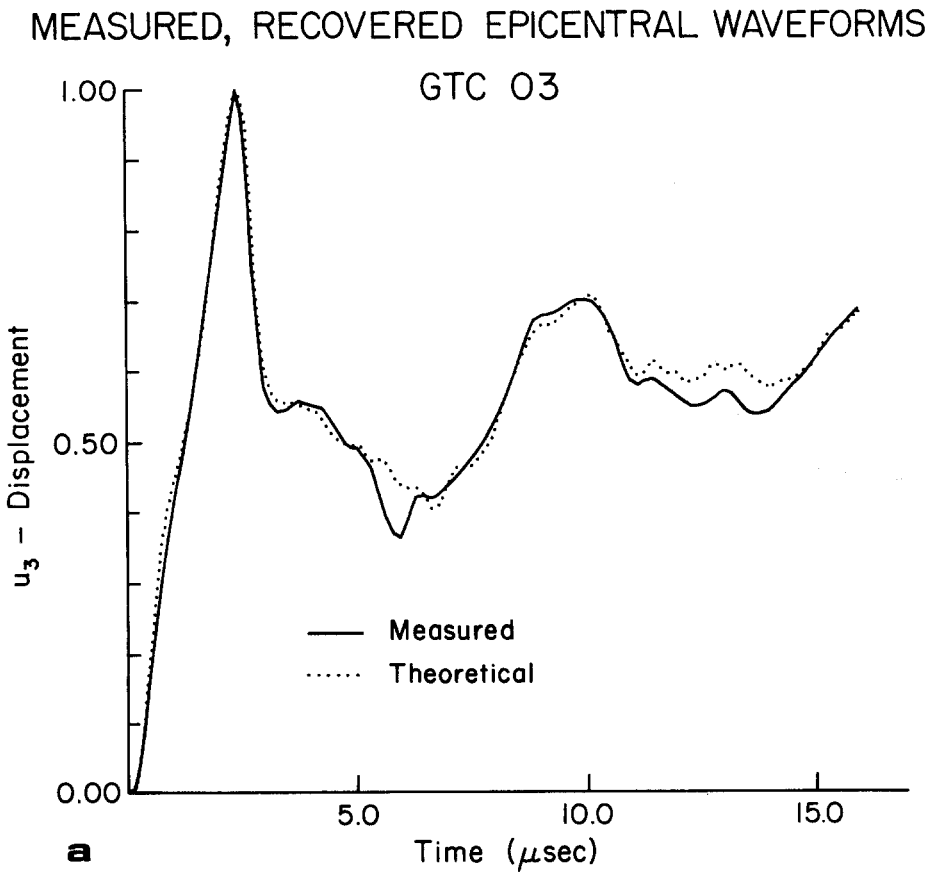

Figure 9(a). Comparison between synthesized and observed signals from GTC 03.

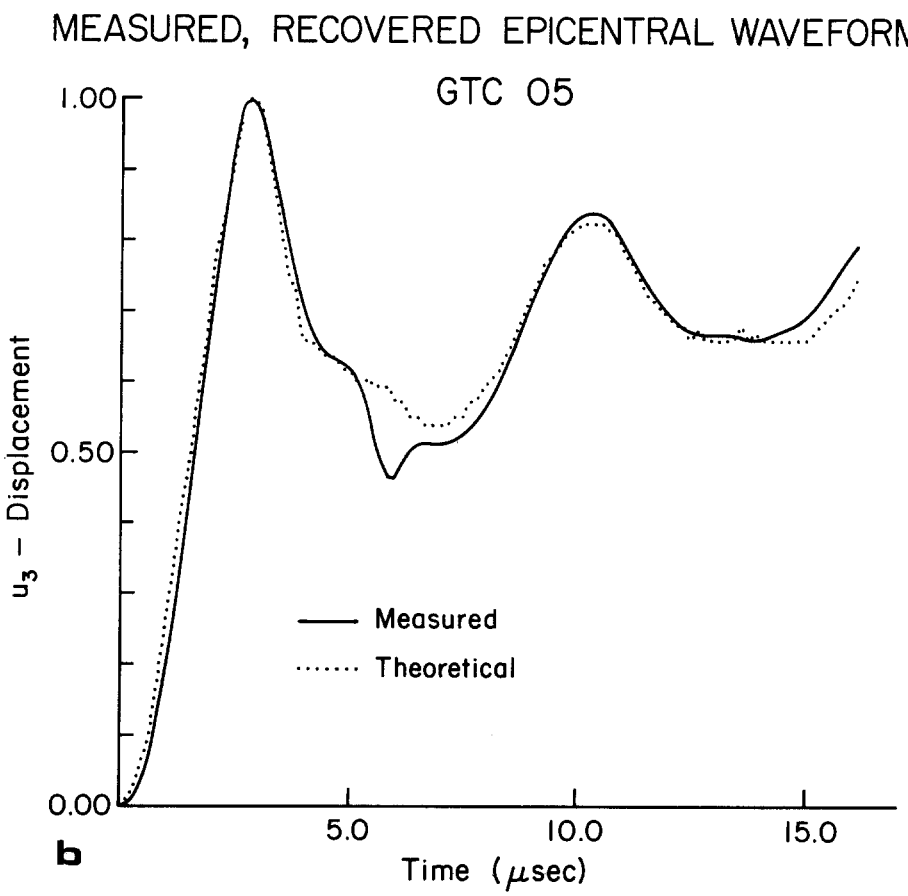

Figure 9(b). Comparison between synthesized and observed signals from GTC 05.

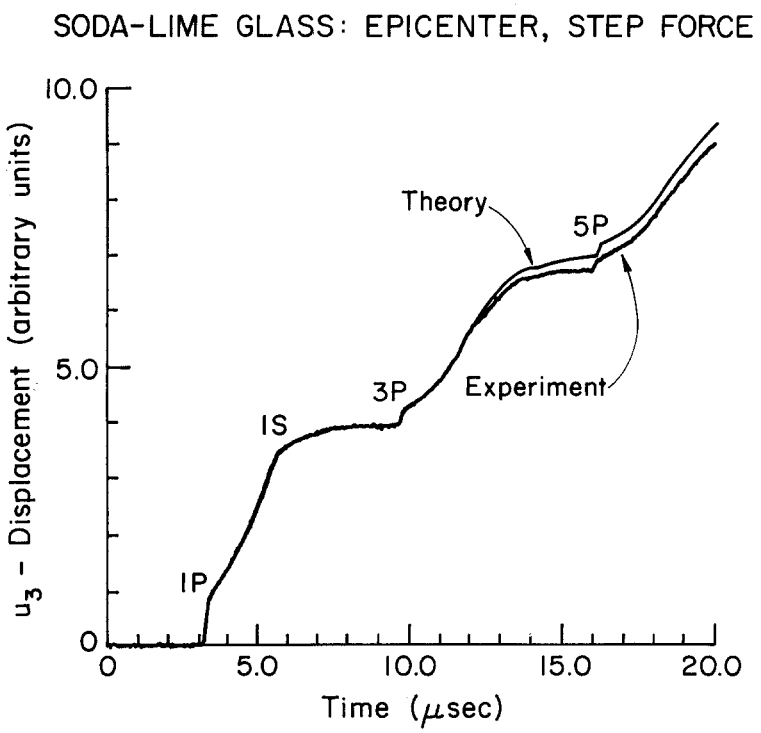

Figure 10. Comparison between synthesized and observed signals from typical glass capillary breaking, GCB 06.

The P-wave travel time through the thickness of the specimen plate is calculated to be 3.19 μsec.

Once the moment tensor and its source-time function were determined, $\hat{u}_3^d(t)$ was calculated [see (3.16)] and compared with $V_0^d(t)$. They are plotted in arbitrary units in Figs. 9(a) and 9(b), respectively, exhibiting excellent agreement between them. The value of $[\hat{u}_3^d/V_0^d]$ in (3.20) was determined by taking an average of 75 discrete data points from the first P-wave arrival over the total time span 6 μsec.

Similar procedures were followed for the analysis of the epicentral response due to the breaking capillaries, using (3.15) and (3.17). A simulated $\hat{u}_3^m(t)$ curve is compared with the experimentally obtained $V_0^m(t)$ in Fig. 10, with both of them plotted in arbitrary units. Agreement between them is seen to be excellent up to the $\sim 5P$-wave arrival. The strength of capillary fracture F_3 ranges from 1.98 N to 2.97 N (see Table 1). $[\hat{u}_3^m/V_0^m]$ in (3.20) was similarly determined for each capillary fracture that preceded the generation of the corresponding thermal crack. The average values of $[\hat{u}_3^m/V_0^m]$ and $[\hat{u}_3^d/V_0^d]$ are both shown in Table 1.

Finally, the strength of a dipole (D_{11}) normal to the crack plane is calculated according to (3.21). It is recorded together with the risetime data of an AE source-time function for nine different thermal cracks in Table 2. Table 1 lists all the relevant data necessary for the determination of the AE source characteristics summarized in Table 2. It is noted that the risetime of an AE source-time function associated with the thermal crack falls between 0.32 μs and 1.75 μs, while the normal dipole stength D_{11} ranges from 0.009 N-m to 0.12 N-m.

5. Discussion

We have demonstrated that a thermal crack AE source generated at (or near) a free surface behaves like that of a crack in plane stress which is, for instance, encountered in a thin plate. In this section we will concentrate on the physical interpretations of a normal dipole (M_{11}) in view of fracture mechanics. The crack model we have chosen for this purpose is a Dugdale-Barenblatt [18,19] thin zone model applied to a thin plate. This model is well suited for the explanation of crack formation in both plastic solids (Dugdale model) and brittle solids (Barenblatt model).

As shown in Fig. 11, we envisage a nonlinear zone surrounding the penny-shaped crack. The size of the thin, nonlinear zone is characterized by l which is much smaller than the characteristic dimensions of the crack a and c. The cardinal nature of the Dugdale-Barenblatt scheme is the laminar geometry of the separation process, consistent with the assumptions adopted in the formulation of Rice's J-integral [20]. Crack growth in this picture is described as the sequential rupture of microstructural linkage units of length l and critical rupture displacement u_c across the crack plane. Across the zone boundary between the outer (linear) and inner (nonlinear) zones is maintained a balance between the distributions of opening and closing stresses. The opening stresses are caused by the spatial temperature gradients and transmitted through the linear material, and the closing stresses, $-\sigma_{11}$, are imposed by the nonlinear material.

The sequential rupture of microstructural linkage units, as the crack front advances, is translated into the drop-out of the closing stresses, $-\sigma_{11}$, on the zone boundary. Denoting the area swept by the crack front by $A(t)$, the normal dipole component, $M_{11}(t)$, can be expressed as

$$M_{11}(t) = \sigma_{11}(t)A(t)l = D_{11}\hat{S}^d(t). \tag{5.1}$$

For ductile (plastic) materials σ_{11} may be replaced by σ_f (flow stress) or σ_y (yield stress).

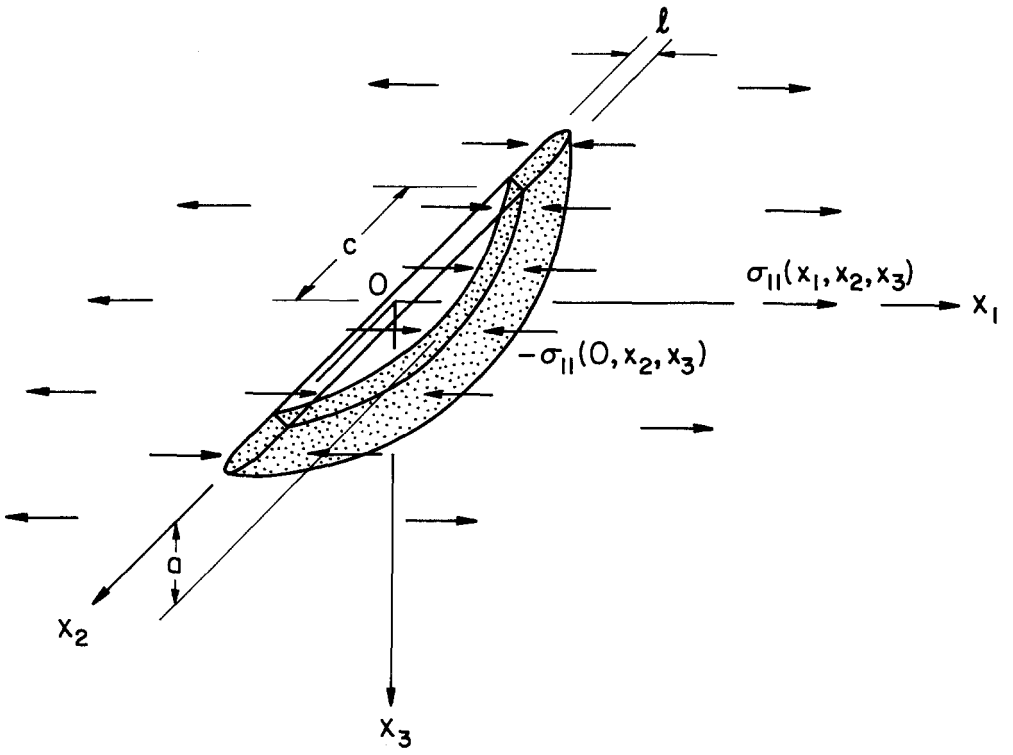

Figure 11. Dugdale-Balenblatt thin zone model for a crack. The dotted region ahead of a crack tip means a nonlinear cohesive zone.

For glass which is very brittle, σ_{11} can be approximated by replacing it with σ_{th}, the theoretical fracture stress of a perfect solid

$$\sigma_{th} \simeq \frac{E}{10} \tag{5.2}$$

where E is the Young's modulus.

Then (5.1) can be written as

$$M_{11}(t) = D_{11}\hat{S}^d(t) \simeq \sigma_{th} A(t) l. \tag{5.3}$$

The Young's modulus of the specimen was measured and found to be 75 GPa. Taking for example GTC 05 (see Table 1) which was observed to have the crack size of $\sim 10^{-5}$ m^2, l is calculated to be about 0.7 μm. For perfectly brittle solids, in which the nonlinear zone essentially vanishes, and to which the Barenblatt model is well adapted, the microstructural linkage units may be identified with cohesive bonds and l thus reduces to the interatomic spacing. Energy release during the formation of a crack in perfectly brittle solids occurs exclusively at the created crack surface and its rate is equal to the surface energy, as the thermodynamic treatment of the original Griffith's [21] model implies.

If we define the source volume of an AE source as Al in (5.1), the source volume for perfectly brittle solids essentially vanishes and the source size is that of a created crack area. The finite value of l in the glass specimen is interpreted as its deviation from perfect brittleness. The size of the small cohesive zone, l, in the context of an AE source may also be called the dipole linkage distance which may be identified as the critical crack opening displacement (COD) at the crack tip. l (or the COD) can thus be taken as a constant independent of time for a given material, as the front of a microcrack advances. Assuming

further that the shape of the advancing crack preserves a geometric similarity (constant ratio between a and c) and the area increment due to a newly created crack is small, one obtains a linear crack velocity $v(t)$

$$v(t) = \frac{dc}{dt} = k_1 \frac{dA(t)}{dt} = k_2 \frac{d\hat{S}^d(t)}{dt}, \tag{5.4}$$

where k_1 and k_2 are constants. The constant k_2 is determined by integrating (5.4), yielding

$$k_2 = \int v(t)\, dt = c_f - c_i = \Delta c, \tag{5.5}$$

where c_i and c_f are the initial and final crack sizes, respectively. With knowledge of the source-time function and the size of the created crack as well, it is possible to determine the crack velocity as a function of time. However, an accurate determination of the shape and size of the generated thermal cracks was not carried out in this experiment and such measurements are left for a subsequent investigation.

Care should be taken in directly applying (5.4) for the calculation of crack velocity in ordinary engineering materials, since they exhibit the effects of frequency dependent attenuation and material dispersion in wave propagation. These effects were not taken into account in the derivation of the source-time function $\hat{S}^d(t)$. Although in glass these effects are small enough for (5.4) to be applicable, they are believed to be quite significant for ordinary engineering materials such as steel. The effect of material damping and frequency-dependent attenuation on the behavior of the epicentral response is under study. Secondly, the effect of an aperture due to the finite size of an AE source and a receiver has to be considered in obtaining the source-time function $\hat{S}^d(t)$. Finally, shown

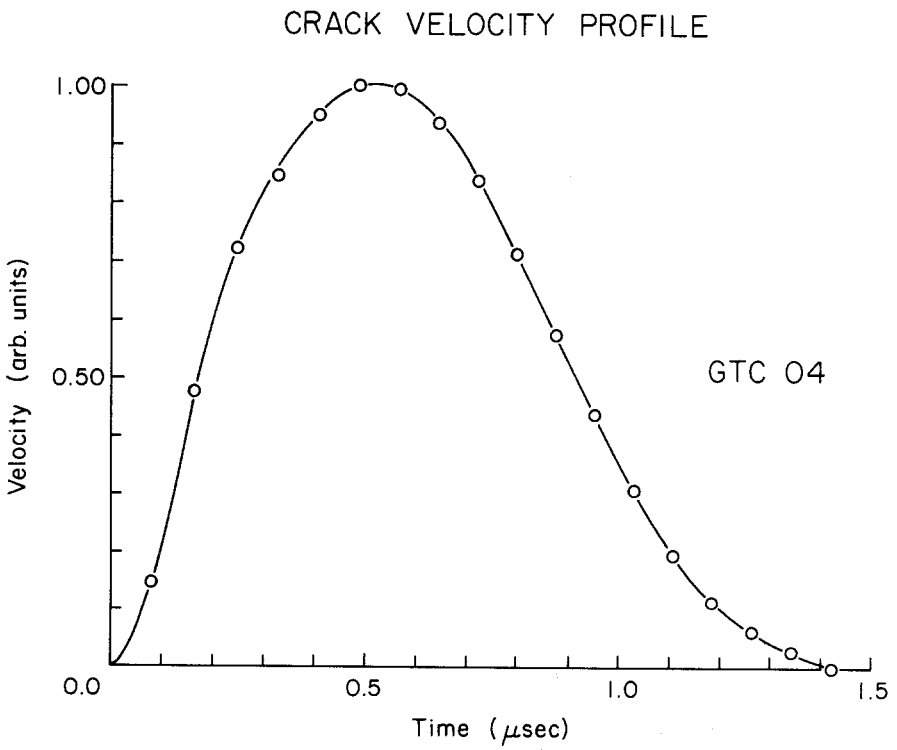

Figure 12. Profile of a crack areal velocity (GTC 04).

in Fig. 12 is the time-derivative of $\hat{S}^d(t)$ of GTC 04, known as the profile of the crack areal velocity. It is seen that the crack velocity initially increases to a peak value and decreases to zero as the crack arrests.

6. Conclusions

Based on our work described here, the following conclusions can be drawn about the nature of the thermal cracks and their AE sources.

(1) The thermal cracks generated under the symmetric cooling at (or near) the free boundary are of mode I type.

(2) The formation of these thermal cracks emits characteristic AE signals reproducibly. Their epicentral response and AE radiation pattern are typical of those of a mode I crack.

(3) The dominant contribution to the AE source of the above cracks comes from a dipole acting normal to the crack plane.

(4) The AE source of a surface crack with a traction-free boundary acts as an AE source in plane stress.

(5) Knowledge of the dipole strength and time function of an AE source can provide useful information on the dynamic behavior of fracture.

Acknowledgement

The financial support of this work by the National Science Foundation through grants to the Materials Science Center and College of Engineering at Cornell University is gratefully acknowledged. The authors express their gratitude to Messrs. S. Howard and W. Pierce for their help with plotting the AE radiation patterns.

References

[1] K. Aki and P.G. Richards, *Quantitative Seismology: Theory and Methods,* Vol. I, Freeman, San Francisco (1980) Chapter 3.
[2] K.Y. Kim and W. Sachse, in *Progress in Acoustic Emission II,* M. Onoe, K. Yamaguchi, and H. Takahashi, Ed., Proceedings of the 7th International Acoustic Emission Symposium, Zao, Japan, October 23-26, Japanese Society for Non-destructive Evaluation (1984) 163–172.
[3] K.Y. Kim and W. Sachse, *Journal of Applied Physics* 59 (1986) 2704–2710; 2711–2715.
[4] L. Knopoff, *Journal of Applied Physics* 29 (1958) 661–670.
[5] N.N. Hsu, J.A. Simmons, and S.C. Hardy, *Materials Evaluation* 35 (10) (1977) 100–106.
[6] Y.H. Pao and R.R. Gajewski, in *Physical Acoustics,* Vol. XIII, W.P. Mason and R.N. Thurston, Ed., Academic Press, New York (1977) 183–265.
[7] A.N. Ceranoglu and Y.H. Pao, *Transactions of ASME* 48 (1981) 125–132; 48 (1981) 133–138; 48 (1981) 139–147.
[8] K.Y. Kim and W. Sachse, *Journal of Applied Physics* 55 (1984) 2847–2856.
[9] W. Nowacki, *Thermoelasticity,* Addison-Wesley, London (1962) 102–113.
[10] F. Gilbert, *Geophysical Journal of the Royal Astronomical Society* 22 (1970) 223–226.
[11] D.J. Doornbos, in *Identification of Seismic Sources-Earthquake or Underground Explosion,* E.S. Husebye and S. Mykkeltvert, Ed., D. Reidel Publishing Co. (1981) 207–232.
[12] G. Bachus and M. Mulcahy, *Geophysical Journal of the Royal Astronomical Society* 46 (1976) 341–361.
[13] G. Bachus and M. Mulcahy, *Geophysical Journal of the Royal Astronomical Society* 47 (1976) 301–329.
[14] A.E.H. Love, *A Treatise on the Mathematical Theory of Elasticity,* Dover Publications, New York, Fourth ed., (1944) 186–189.
[15] P.M. Morse and H. Feshbach, *Methods of Theoretical Physics,* McGraw-Hill, New York (1953) Part I, Chapter 7.
[16] G. Bachus, *Geophysical Journal of the Royal Astronomical Society* 51 (1977) 1–25; 51 (1977) 27–45.
[17] J.E. Michaels and Y.H. Pao, *Journal of the Acoustical Society of America* 77 (1985) 2005–2011.
[18] D.S. Dugdale, *Journal of the Mechanics and Physics of Solids* 8 (1960) 100–104.
[19] G.I. Barenblatt, *Advances in Applied Mechanics* 7 (1962) 55–129.
[20] J.R. Rice, *Journal of Applied Mechanics* 35 (1968) 379–386.
[21] A.A. Griffith, *Philosophical Transactions of the Royal Society,* London, A221 (1920) 163–198.

Résumé

On a créé des fissures thermiques de Mode I orientées normalement à une surface en projetant de l'azote froid par un petit ajustage sur une rainure initiale à la surface d'une plaque de verre. Les signaux d'émission acoustique émis par la fissure thermique ont été détectés sur la face opposée de la plaque, à l'épicentre et en d'autres positions par rapport à la fissure, en utilisant un système de captation à neux canaux. Les formes d'ondes détectées fournissent les caractéristiques de la source acoustique, telles que les composantes du tenseur de moment, la fonction sourcetemps, la répartition de la radiation et la puissance du dipole. Cette dernière grandeur a été déterminée, lorsqu'elle est associée aux fissures thermiques, en comparant les signaux obtenus à ceux que produit un capillaire de verre rompu à l'endroit de la fissure, avant que celle-ci se forme. On montre que la fonction d'émission acoustique source-temps ainsi que la puissance dipole peuvent fournir des informations valables sur le comportement dynamique d'une rupture.